Received: 19 October 2020 | Revised: 13 May 2021 | Accepted: 16 May 2021

DOI: 10.1111/jace.17934

Journal of the American Ceramic Society

ORIGINAL ARTICLE

# Comparison of different sintering aids in cold sinter-assisted densification of lead zirconate titanate

**Shruti Gupta** | **Dixiong Wang** | **Clive A. Randall** | **Susan Trolier-McKinstry**

Department of Materials Science and Engineering and Materials Research Institute, The Pennsylvania State University, University Park, PA, USA

**Correspondence**
Shruti Gupta, Department of Materials Science and Engineering and Materials Research Institute, The Pennsylvania State University, University Park, PA 16802, USA.
Email: sxg628@psu.edu

**Funding information**
National Science Foundation, Grant/Award Number: IIP-1841453 and IIP-1841466

**Abstract**

Ceramics such as lead zirconate titanate (PZT) tend to dissolve incongruently, and thus pose a challenge in the cold sintering process. Moist lead nitrate has previously been shown to enable a cold sinter-assisted densification of PZT by a viscous phase sintering mechanism. In this paper, lead acetate trihydrate is demonstrated to lower the required temperature of the cold sintering step to 200°C. This densification process was described as a two-step process: cold sintering of PZT with lead acetate trihydrate and post-annealing the as-cold sintered PZT ceramics. Unlike in the case of lead nitrate, PZT densification with lead acetate trihydrate occurs by a liquid phase assisted sintering mechanism, leading to an as-cold sintered relative density of 84% at 200°C. After performing a post-anneal step at 900°C, >97% relative densities were achieved in samples that were cold sintered with lead acetate trihydrate. This step not only densified PZT but also refined the grain boundaries. In the post-annealed samples, the room-temperature relative permittivity at 100 Hz was ~1600, slightly higher than that reported in samples that used lead nitrate as a sintering aid; the loss tangent was about 3.8%. For measurements at 10 Hz, the remanent polarization in both cases was ~28 μC/cm$^2$. Both Rayleigh analysis and aging studies showed that a higher irreversible contribution to the permittivity exists in samples that used lead nitrate as a cold sintering aid.

**KEYWORDS**

electroceramics, lead zirconate titanate, piezoelectric materials/properties, processing, sinter/sintering

## 1 | INTRODUCTION

Various processing methods such as hydrothermal sintering,[1] spark plasma sintering,[2,3] microwave sintering,[4] liquid phase sintering,[5] and cold sintering[6] have been developed in an effort to lower sintering temperatures for bulk ceramics. In many of these approaches, a secondary liquid phase, often called a sintering aid, is used to lower processing temperatures significantly[7–9] via a liquid phase sintering mechanism. For example, compounds such as $Cu_2O$/PbO, $V_2O_5$, $P_2O_5$, or $LiBiO_2$ facilitate densification of lead zirconate titanate (PZT) ceramics at <1000°C; without such liquid phases, PZT is typically sintered at 1200–1300°C.[10–13]

Gutmanas et al.[14] first coined the term "cold sintering" in 1983 to refer to a plastic deformation in metals at low temperatures by utilizing extremely high uniaxial pressure: ~GPa's. Recently, the cold sintering process (CSP) has enabled densification of a number of ceramic materials at temperatures of 25–300°C in the presence of a transient liquid phase and applied uniaxial pressure: ~100 to 500 MPa (in an open system).[15] A broad range of material chemistries and material structures including metal oxides,[16] inorganic salts,[17] composites,[18,19] and multilayer systems[20] have been

  

densified using this approach, enabling preparation of prototyped varistors,[21] battery materials,[22] capacitors,[23] and piezoelectric actuators and sensors,[24,25] etc.

As in liquid phase sintering, the CSP occurs as a result of particle rearrangement, dissolution-precipitation mechanisms, and grain growth, albeit in the presence of a *transient* liquid phase.[15] Ideally, the sintering aid provides a transient phase which partially dissolves the ceramics, promotes particle rearrangement, and allows precipitation of the supersaturated solution at the pores as the transient phase evaporates. Often, the sintering aids used are water-soluble polar inorganic salts. The most commonly used solvent in cold sintering is water; however, other ionic and organic liquids are also utilized. In cold sintering inorganic composites, a low solubility ceramic can be cold sintered with a high solubility salt containing cations of interest.[26] This salt helps lubricate the ceramic particles such that particle rearrangement is enhanced, and high green densities are obtained.

The role of moisture in lowering the sintering temperature of certain metal oxides and sulfates was first studied in the 1950s.[27] More recently, Kähäri et al.[28,29] demonstrated that the addition of water to $Li_2MoO_4$ can promote its densification near room temperatures under applied uniaxial pressure. Since cold sintering is carried out in an open system, the moisture present in the surrounding air plays a critical role as an additional transient phase. Floyd et al.[30] concluded that increasing the relative humidity from 24% to 54% at room temperature leads to a 10% rise in the relative density of cold sintered ZnO.

Wang et al.[31] recently reported a model for densification of PZT by a cold sinter-assisted process using moistened lead nitrate as the sintering aid. This model assumes that plastic deformation of lead nitrate leads to viscous phase sintering, resulting in a relative density of 89% following the cold sintering step at 300°C and 500 MPa uniaxial pressure. In their experiments, water was utilized as a solvent for lead nitrate to assist in the initial particle rearrangement. However, due to limited control of the water evaporation rate, this procedure can produce varied results depending on the amount of residual water available for densification during CSP.[28]

To circumvent this problem, salts containing structural water, molten hydroxide fluxes, and hydrofluxes have been explored as sintering aids. The eutectic mixture of NaOH and KOH at 170°C can be used to lower the synthesis temperature of various complex oxides.[32,33] For example, Tsuji et al.[34] have employed this alkali flux in a one-step cold sintering process for $BaTiO_3$ at temperatures as low as 300°C in 12 h at 520 MPa. Sada et al.[35] have shown that by using transient chemistry such as a $Ba(OH)_2$ octahydrate, the densification of $BaTiO_3$ by cold sintering can occur at a significantly reduced temperature and time of 225°C and 1 h. Recently, several chemical pathways for cold sintering have been described wherein upon cold sintering, the final product either: (1) retains the chemical composition or phase of the starting powders (e.g., ZnO, magnetite), (2) has a different chemical composition or phase than the starting powders (e.g., α-quartz), or (3) results in a new compound or chemical doping (e.g., $BaTiO_3$ cold sintered with $BaOH_2{\cdot}8H_2O$ or $SrOH_2{\cdot}8H_2O$).[36] In this work, lead acetate (PbAc) trihydrate is explored as a sintering aid to densify PZT by CSP. This approach is "water-free" in that only the structural water is used in the densification process. Residual PbAc also serves as a lead source during the post-anneal to complete densification. This paper determines the limits of densification by cold sintering PZT with lead acetate trihydrate as a sintering aid and compares densification mechanisms and dielectric properties with previous work on cold sintering of PZT with lead nitrate.[25]

## 2 | EXPERIMENTAL PROCEDURE

### 2.1 | Densification of PZT

In this work, densification of PZT is described as a two-step process.

#### 2.1.1 | Step 1: Cold sintering of PZT with lead acetate trihydrate (PbAc trihydrate)

CSP with PbAc trihydrate as the sintering aid at varying pressures and temperatures was studied in order to determine the densification mechanism during the process. For this purpose, PZT-5A (PKI-509, Piezo Kinetics, Inc.) of ~3 μm average particle size was attrition milled to ~400 nm average particle size and combined with a sol–gel derived soft PZT powder of ~100 nm particle size by a process described elsewhere.[25] For a single pellet, 0.5 g of this PZT powder was combined with 0.035 g (~15 vol%) of lead acetate trihydrate powder (Sigma-Aldrich Corp., purity ≥99.99%, density 2.55 g/cm$^3$) and hand-ground in a mortar and pestle to homogenize the mixture. This composition provided: (1) low residual PbO in the grain boundaries upon post-anneal, (2) no extrusion of material from the die due to excess liquid phase, and (3) sufficient liquid phase to wet the PZT particles. This powder mixture was then transferred into a cylindrical die (Wartburg Tool & Die, Inc.) with a 1.27 cm inner diameter and pressed at uniaxial pressures of 100–500 MPa. Each experiment was conducted for 3 h at different temperatures (50, 100 150, 200, 250, 280, and 290°C). Pellet densities were measured using the geometric method.

In order to understand the decomposition process at different cold sintering temperatures, two batches of PbAc trihydrate powder were heated in air at ambient pressure conditions at either 200 or 290°C. The decomposed phases were identified

using X-ray diffraction (XRD, Empyrean, PANalytical Corp.) with Cu Kα radiation. Scans were taken from 2θ = 5° to 70° with a step size of 0.026° 2θ and a scan rate of 0.067°/s. Using a Simultaneous DSC/TGA (SDT, TA Instruments Q600), the melting point and decomposition of PbAc trihydrate were also measured by heating the powder from room temperature to 400°C at a continuous ramp rate of 20°C/min in air.

#### 2.1.2 | Step 2: Post-annealing the cold sintered PZT parts

Post-annealing of the cold sintered samples was carried out in a box furnace using a ramp rate of 5°C per minute to 900°C with a 3 h hold time at 900°C, prior to furnace cooling.

For grain size measurement, the samples were polished using 15, 9, 6, 3, and 1 μm diamond polish successively using a rotation speed of 200 rpm. The average grain size was calculated using the linear intercept method described by Equation (1)[37]:

$$\text{Average grain size} = 1.5 \times \frac{\text{total length of lines}(\mu\text{m})}{\text{total grain boundary count}} \quad (1)$$

## 3 | DIELECTRIC MEASUREMENTS

The following samples were used to investigate dielectric and piezoelectric properties:

1. PZT cold sintered with Pb acetate trihydrate at 200°C for 3 h at 500 MPa and post-annealed at 900°C for 3 h.
2. PZT cold sintered with Pb nitrate at 300°C for 3 h at 500 MPa and post-annealed at 900°C for 3 h.

These samples were electroded by sputter depositing silver on the front and back surfaces. The dielectric permittivity and loss tangents were measured using a Hewlett-Packard 4284A LCR meter (Agilent Technologies, Inc.). A system with a Trek Model 30/20 high voltage amplifier system (Trek, Inc.) and LabVIEW software (National Instruments Corporation) was used to measure the polarization-electric field hysteresis loops (P-E loops) at room temperature at 10 Hz. The same system was used for DC poling the samples at 35 kV/cm for 1 h at room temperature.

## 4 | RESULTS AND DISCUSSION

### 4.1 | Densification of PZT

#### 4.1.1 | Step 1: Cold sintering of PZT with lead acetate trihydrate (PbAc trihydrate)

Cold sintering experiments were conducted to determine the dependence of final cold sintered density on the applied uniaxial pressure. A series of experiments was carried out using a cold sintering temperature of 200°C for 3 h. It was observed that increasing pressure yielded a monotonic increase in relative density, as shown in Figure 1A. The maximum pressure applied (500 MPa) yielded a maximum relative density of ~84%. The relative densities were calculated by normalizing the as-cold sintered densities to the theoretical density of PZT (7.8 g/cc).

It is clear in Figure 1B that the as-cold-sintered PZT composite density showed a non-monotonic trend as a function of temperature, where the as-cold-sintered density underwent a maximum as a function of cold sintering temperature, with the peak relative density occurring near a CSP temperature of 200°C. This behavior could be related to the phase changes that occur in PbAc trihydrate which cause a change in densification mechanisms at different CSP temperatures. To understand the difference in the densification mechanisms with CSP temperature, the following regions have been considered: (1) Below ~60°C: PbAc trihydrate retains

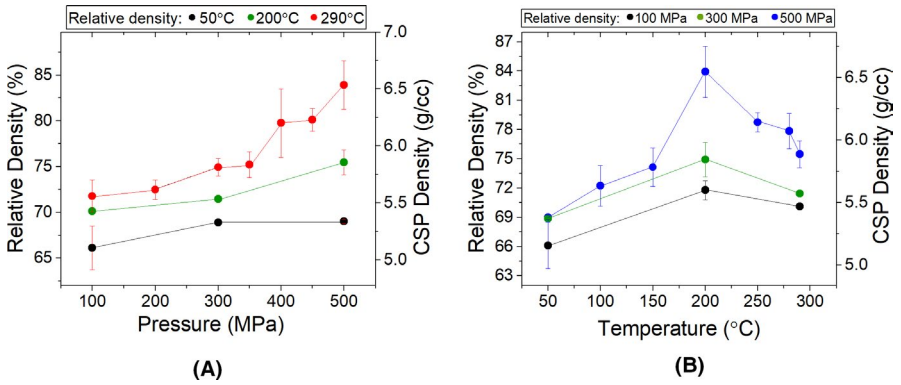


**FIGURE 1** As-cold sintered density as a function of (A) pressure and (B) temperature during the cold sintering step. All experiments were carried out for 3 h. Error bars show the standard deviation of the densities; variability in the measured densities may be due to the change in the ambient relative humidity. In both figures, the lines are guides to the eye

its solid crystalline form at ambient pressures (Figure S2), (2) Between ~60 and ~200°C: PbAc trihydrate progressively loses its water of hydration and melts, (3) By 200°C: lead acetate exists in an anhydrous form (Figures S1a and S2), and (4) >250°C: lead acetate decomposes (Figure S2).[38]

To probe these different regimes, dilatometry was carried out at cold sintering set temperatures of 50, 200, 250, and 290°C. To do this, the temperature ramp was started, then the pressure was applied. Typically, the pressure stabilized within approximately 2 s; the time at which the pressure stabilized was treated as time zero. Depending on the set temperature, the desired temperature was reached within a few minutes. The linear contraction was measured during uniaxial pressing using a setup designed by Floyd et al.[39] Figure 2 is a comparison of the percent contraction data for the PZT/PbAc trihydrate composite during cold sintering. Given the fixed radius of the die, the measured linear contraction ($\Delta L$) (i.e., the thickness reduction of the sample) is the same as its volume contraction. Thus, a larger $\Delta L$ corresponds to a higher density. The percent thickness reduction was calculated from $\Delta L$ and the initial thickness of the powder bed ($L_0$), as shown in Equation (2):

$$\%\ \text{thickness reduction} = \frac{\Delta L}{L_0} \times 100 \tag{2}$$

The dilatometer was set to collect data every 5 s starting from the point when the set pressure was reached. From Figure 2, it is apparent that there is initial rapid densification, probably due to particle rearrangement, with plateaus to different densities.

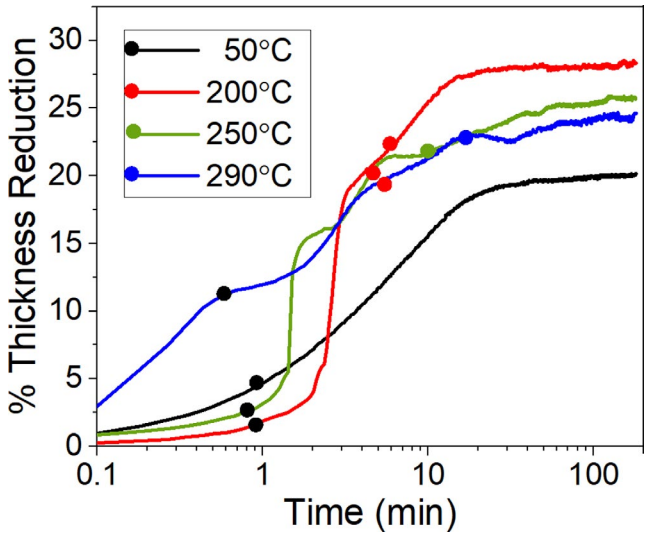


**FIGURE 2** Percent thickness reduction of the powder bed as a function of cold sintering process time. The line color denotes the setting temperature of the die during cold sintering. The dots mark times at which particular temperatures were reached. For example, the red dot on the blue curve indicates when a die temperature of 200°C was reached

PbAc trihydrate melts at ~60°C and progressively loses the waters of hydration, as shown by the SDT thermogram in Figure S2. It is evident from Figure 1B that the as-cold sintered densities below this temperature are the lowest, as only particle packing occurs between the PZT and the PbAc trihydrate grains. This corresponds to an ~18% reduction in thickness, as seen in Figure 2. The resulting microstructure of the as-cold sintered part is shown in Figure 3A. PbAc trihydrate crystals occupy areas between PZT grains as is expected during dry pressing.

The melting of PbAc trihydrate produces higher as-cold sintered densities above ~60°C by providing a liquid phase that assists in particle rearrangement via lubrication of the PZT grains and pore filling due to capillarity. As described by Svoboda et al.,[40] the rate of densification due to particle rearrangement is driven by two factors: the capillary forces exerted on the solid grains by the liquid phase and any mechanical pressure existing at the points of contact between the solid grains. These factors provide an unbalanced force that drives further densification to a solid obtained by random dense particle packing in the absence of a liquid phase.[40] Even though PbAc trihydrate begins to melt at ~60°C at ambient pressures, a steep increase in as-cold sintered density is observed between cold sintering temperatures of 150 and 200°C in Figure 1B. As shown by Svoboda et al.,[40] the rate of densification due to particle arrangement varies inversely with the liquid viscosity. Given that viscosity decreases exponentially with increasing temperature, it is possible that the increases in densification are due to improved particle rearrangement in the presence of the liquid phase. Moreover, under ambient pressure conditions, lead acetate is anhydrous at 200°C (Figures S1a and S2).[38] It is possible that as the structural water is released progressively, it further decreases the viscosity of the liquid phase, aiding densification.

The highest reduction in thickness of ~28% was obtained for samples cold sintered at 200°C. In Figure 2, the black dot on the red curve indicates the time when the temperature of 50°C was reached. A change in slope at about 2 min indicates the melting of lead acetate (>70°C). Another slight change in slope occurs at 6 min, at which point the die temperature reached 200°C. The densification continues even after the set temperature was reached. As seen in the densification curve for samples cold sintered at 200°C in Figure 2, even though a die temperature of 200°C is reached within the first 6 min (indicated by the red dot on the red curve), significant thickness reduction occurs up to cold sintering times of 11 min, after which the curve plateaus. Figure 3B shows the microstructure of the as-cold sintered PZT at 200°C. The resolidified Pb acetate occupies areas around the PZT grains.

A decrease in ceramic density is observed for cold sintering temperatures above 200°C. A continuous decomposition of lead acetate occurs at temperatures above 250°C (Figure S2).[38] Thus, during cold sintering in this temperature range, there is reduced pore filling and lubrication of PZT particles

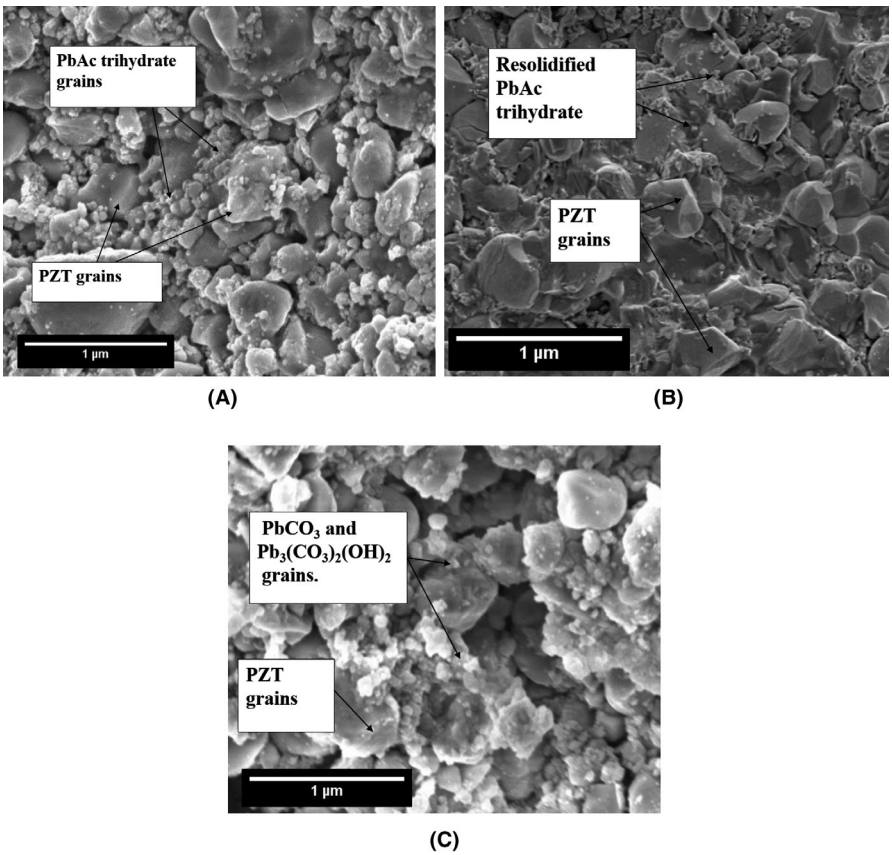


**FIGURE 3** SEM images showing (A) Pb acetate trihydrate crystals accumulated between larger PZT grains after cold sintering at 50°C. (B) resolidified Pb acetate particles between PZT particles when cold sintering was performed at 200°C. (C) PZT particles with decomposed lead acetate particles when cold sintered at 290°C

provided by the available liquid phase. This leads to a ~25% thickness reduction in samples that were cold sintered at 250°C as seen in Figure 2.

When cold sintering PZT at 290°C, the time period for which sintering aid remains molten as lead acetate (e.g. before the temperature rises to the point at which it starts to decompose, ~10 min) is far less than for the case when PZT is cold sintered at 200°C (180 min). As the molten lead acetate decomposes, lubrication of the PZT grains is reduced. In other words, there is an insufficient amount of time for the liquid phase to facilitate adequate particle rearrangement; this leads to low densities in these samples. The densification curve in Figure 2 saturates at 18 min when the die temperature reached 290°C. The thickness reduction was ~24%. At this temperature, the decomposed phases are identified as $PbCO_3$ and $Pb_3(CO_3)_2(OH)_2$ using X-Ray diffraction as shown in Figure S1c. The microstructure in Figure 3C indicates this decomposed phase around the PZT grains.

This shows that the densification of PZT during the cold sintering step is determined by the phase of the sintering aid at the cold sintering conditions. It is presumed that the dominant densification mechanism for CSP of PZT with PbAc trihydrate at 200°C is a liquid phase-assisted particle rearrangement.

Wang et al.[31] studied cold sintering of PZT ceramics with lead nitrate as a sintering aid. In the initial stages of pressing, particle rearrangement led to rapid densification. As a control, if no lead nitrate was added, the densification was limited to some particle rearrangement, and therefore the compact is not considered to undergo a sintering process. However, with lead nitrate, additional densification could be well described as viscous sintering based on the assumption that lead nitrate undergoes plastic deformation under the applied pressure and temperature during CSP. A viscous phase sintering model was developed for that system that described the late stages of densification. Murray et al.[41] proposed that for viscous sintering, the density ($\rho$) varies exponentially with applied pressure ($\sigma$) according to the equation:

$$\rho = 1 - e^{\left(-\frac{3\sigma}{4\eta}\right)t + c} \tag{3}$$

where, $\eta$, $t$, and $c$ are viscosity, time, and the integration constant, respectively.[41] Both the Vogel–Fulcher–Tamman and an Arrhenius relationship between temperature and viscosity described the available data well.

Using PbAc trihydrate as a PZT sintering aid, it was found that the pressure dependence of the densification can be described either with the viscous phase sintering model[31,41] or the liquid phase sintering model as seen in Figure 4A.[42,43] Therefore, the pressure dependence of the relative density alone cannot be used to determine the densification mechanism. However, as shown in Figure 4B, the density dependence on CSP temperature does not fit a viscous phase

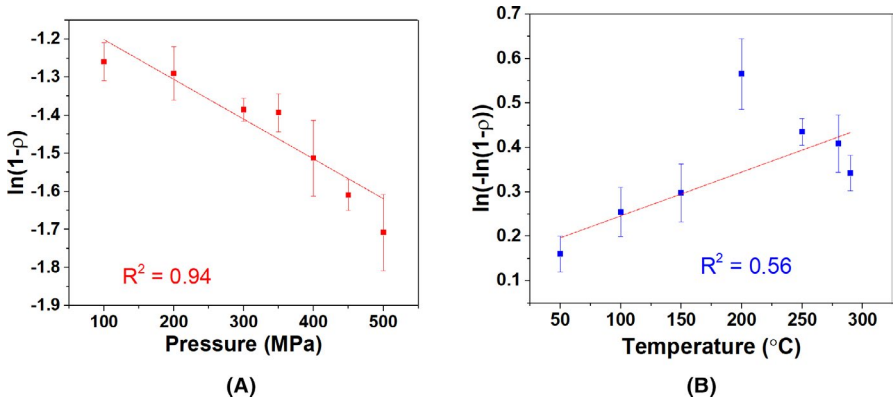


**FIGURE 4** Density variation with applied uniaxial pressure and temperature. The dots are an average of the experimental data points, the error bars are the standard deviation of this data, and the line is the best-fit to the data. (A) The pressure dependence on density (at CSP temperature of 200°C) agrees with the model. However, the temperature dependence (B) is not described by the simple viscous sintering model given that PbAc trihydrate dehydrates, melts, and ultimately decomposes over the cold sintering temperature range studied

sintering model at temperatures >200°C due to the phase changes and decomposition occurring in the sintering aid. Presumably, particle rearrangement and pore filling contribute to densification during cold sintering of PZT with PbAc trihydrate. According to Felten,[42,43] particle rearrangement is a dominant mechanism in the initial stage of densification during uniaxial pressing. The observation that the densification at 200°C is the highest suggests that a liquid phase sintering aid increases particle packing due to increased capillarity and lubrication.

This liquid phase is lost due to the decomposition of PbAc trihydrate above 250°C, causing lower densities. The densities are the lowest below ~60°C, which is consistent with the suggestion that the liquid phase plays an important role in PZT particle rearrangement.

In comparing Figure 4 with work done by Wang et al.,[31] it can be seen that PZT cold sintered at 200°C, with either lead nitrate or PbAc trihydrate, can reach a relative density of ~84%. Since the viscous phase mechanism is enhanced at higher temperatures, PZT-Pb nitrate composites can reach a relative density of 89% at 300°C when cold sintered with 15 vol% lead nitrate. With Wang et al.[31] conducting their dilatometry studies at room temperature, no definitive comparison can be made between the two sintering aids based on dilatometry.

### 4.1.2 | Step 2: Post-annealing the cold sintered PZT parts

As seen from the trends in the data shown in Figure 5, higher cold sintered densities lead to higher PZT packing densities. By increasing PZT packing density, the diffusion distance between the PZT grains is reduced during the post-anneal step. Therefore, as expected, high cold sintered densities corresponded to high post-anneal densities. On post-annealing samples cold sintered using PbAc trihydrate as the cold sintering aid at 50, 200 and 290°C, the final densities obtained were 82.1% ± 1.8%, 97% ± 2.8%, and 86% ± 0.97%, respectively, as indicated in Figure 5.

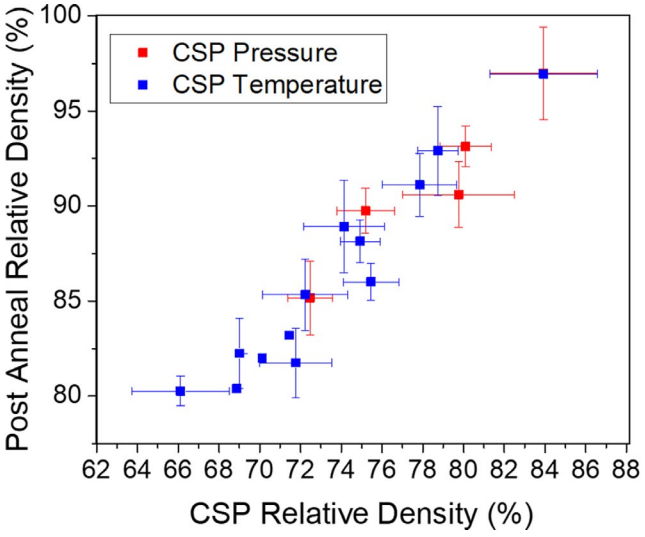


**FIGURE 5** Relative densities of all PZT samples after the post-anneal step plotted as a function of CSP relative densities. Relative densities evaluated by normalizing all measured densities to the theoretical density of PZT (7.8 g/cc). The data points come from the CSP temperature and pressure studies

Figure 6A shows the microstructure of the post-annealed sample that was cold sintered at 200°C at 500 MPa. PbAc trihydrate is fully decomposed into lead oxide above 376°C at ambient pressures (also Figure S2).[38] Since PbO melts at 880°C, at the post-anneal temperature of 900°C, PbO acts as the liquid phase promoting mass transport, and PZT is fully densified by liquid phase sintering. Since the major

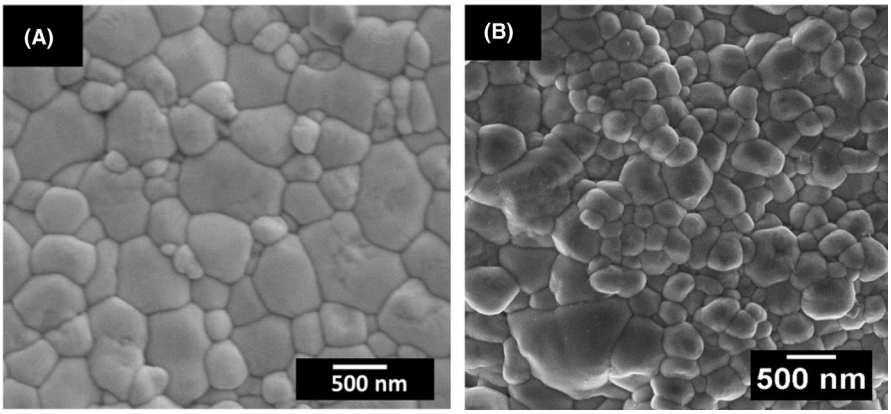


**FIGURE 6** SEM microstructures taken after post-annealing at 900°C samples that were cold sintered (A) using PbAc trihydrate at 200°C and (B) using Pb nitrate at 300°C

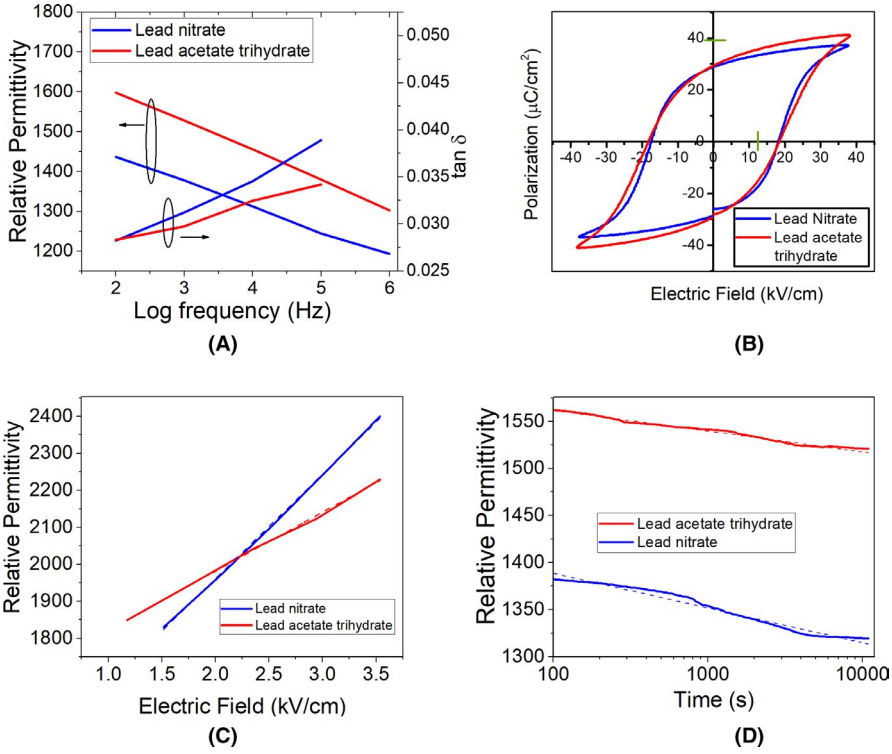


**FIGURE 7** Comparison of dielectric properties of post-annealed samples cold sintered with PbAc trihydrate at 200°C or lead nitrate at 300°C. (A) Relative permittivity and loss tangent as a function of frequency at room temperature. (B) P-E hysteresis loops at 10 Hz performed at room temperature. The green lines on the *y*-axis and the *x*-axis indicate the remanent polarization and coercive field respectively for a conventionally sintered bulk PZT ceramic. The average data from three samples are plotted in (A) and (B). (C) Relative permittivity as a function of AC field in the Rayleigh region at room temperature and 100 Hz for representative samples cold sintered with different sintering aids. (D) Room-temperature measurements of relative permittivity as a function of time measured at 100 Hz after poling at room temperature at 35 kV/cm for 1 h. Dashed lines indicate the linear fitting of each curve in (C) and (D)

byproduct of the decomposition of lead nitrate at 470°C is also a PZT-PbO composite,[44] the densification mechanism in the post-anneal step should be identical in both cases. Figure 6B shows the microstructure of a post-annealed sample that was cold sintered at 300°C with Pb nitrate (98.1% relative density). The powders used were the same in both cases, however, some grains in Figure 6A are slightly larger than those in Figure 6B. The average grain size calculated for samples cold sintered with PbAc trihydrate and lead nitrate was 498 and 409 nm, respectively.

## 4.2 | Dielectric properties

Figure 7A shows relative permittivity and loss tangent as a function of frequency for post-annealed samples that used PbAc trihydrate and Pb nitrate as sintering aids. The relative permittivity and loss tangent were also measured for the as-cold sintered samples (Figure S3). It was found that for post-annealed samples, ceramics cold sintered using PbAc trihydrate showed a higher relative permittivity and lower loss tangents than those cold sintered with Pb nitrate.

**TABLE 1** Rayleigh coefficients and percent extrinsic contribution extracted from a linear fit of the data in Figure 7C. Aging rate for the relative permittivity extracted from Figure 7D. $\varepsilon_{initial}$ is expressed as a range denoting sample-to-sample variations

| | Rayleigh coefficients | | | Aging rates (A) | |
|---|---|---|---|---|---|
| | $\alpha$ (cm/kV) | $\varepsilon_{initial}$ | Extrinsic contribution (at 3 kV/cm) | $\varepsilon_r$ | $d_{33}$ |
| PZT samples that used Pb Nitrate as the cold sintering aid | 289 ± 4 | 1100–1400 | 39% | 2.5% per decade | 3% per decade |
| PZT samples that used PbAc Trihydrate as the cold sintering aid | 161 ± 3 | 1500–1700 | 23% | 1.3% per decade | 2.1% per decade |

However, in both cases, the remanent polarization and coercive field had similar values as seen in Figure 7B.

In order to assess domain wall contributions to the properties at small AC electric fields, Rayleigh analysis was carried out by measuring the relative permittivity as a function of AC field (Figure 7C) at 100 Hz.[45] The irreversible ($\alpha$) and reversible ($\varepsilon_{initial}$) Rayleigh coefficients were extracted from the data in Figure 7C using:

$$\varepsilon_{33} = \alpha E_0 + \varepsilon_{initial} \quad (4)$$

where $\alpha$ and $\varepsilon_{initial}$ are the irreversible and reversible Rayleigh coefficients and $E_0$ is the peak amplitude of the applied electric field.[46] $\varepsilon_{initial}$ includes both lattice and reversible domain wall contributions; the $\alpha E_0$ term comes from irreversible domain wall displacement. The percent of extrinsic contribution was determined using the highest field data and Equation (5)[46]:

$$\%\ \text{Extrinsic contribution} = \frac{\alpha E_0}{\varepsilon_{33}} \times 100 \quad (5)$$

Extrinsic contributions arise predominantly from the motion of domain walls in PZT ceramics. From Table 1, it can be seen that samples that used $Pb(NO_3)_2$ as a sintering aid have a larger extrinsic contribution to the relative permittivity at 3 kV/cm. In samples that used PbAc trihydrate as a sintering aid, a larger fraction of the total relative permittivity comes from the reversible mechanism.

The aging of these samples was studied. The domain state of the samples was perturbed by DC poling at room temperature at 35 kV/cm (~2 times the coercive field) for 1 h. In ferroelectric materials, aging occurs as the domain state gradually approaches local equilibrium after an excitation.[45,47,48] Thus, a faster aging rate can be characteristic of material with either larger domain wall mobility and/or where there is a larger driving force for the domains and domain walls to be pinned.

The rate of change of relative permittivity as a result of aging is described by the following equation[48]:

$$\frac{\varepsilon(t) - \varepsilon(t_0)}{\varepsilon(t_0)} = \frac{A}{100} \log\left(\frac{t}{t_0}\right) \quad (6)$$

where $A$ is the aging rate per decade; $\varepsilon\left(t_0\right)$ refers to the relative permittivity at unit time $t_0$ (100 s in this study) and $\varepsilon(t)$ is the relative permittivity at time $t$ after poling. The aging rates for the cold-sintered PZT ceramics from Figure 7D are listed in Table 1.

Aging was also studied using the piezoelectric coefficient, $d_{33}$, as a function of time measured using PiezoMeter system (PM 300, Piezotest Pte. Ltd.) as shown in Figure S4. The data are shown in Table 1. It must be noted that these values are a result of room temperature poling at two times the coercive field. However, when the samples were poled at 120°C for 1 h at 2.2 times the coercive field, a $d_{33}$ of 310 pC/N was obtained.

The samples with lead nitrate as a sintering aid show larger irreversible contributions to the permittivity, as well as larger aging rates. These two observations would be consistent with a potential energy distribution that has a significant population of smaller energy barriers, relative to PZT ceramics cold sintered using PbAc trihydrate as a sintering aid. It is not clear what the microstructural origin of such pinning sites is, as the average grain size is larger for the samples cold sintered with PbAc trihydrate. Since the number of defects should be inversely proportional to the Rayleigh coefficient α, this suggests that grain boundaries may not be the origin of the pinning for these samples.[49]

## 5 | CONCLUSIONS

Lead acetate trihydrate was introduced as a "water-free" sintering aid for cold sinter-assisted densification of PZT ceramics. The highest as-cold-sintered relative densities were achieved using a cold sintering temperature of 200°C. Unlike cold sintering with lead nitrate, it was shown that PZT with PbAc trihydrate does not follow a viscous phase sintering mechanism during cold sintering due to the phase changes PbAc trihydrate undergoes with increasing temperature. Upon post-annealing at 900°C, PZT relative densities of >97% were obtained in the samples that were cold sintered with Pb acetate trihydrate. These samples showed high relative permittivity values (1500–1700) and low loss tangents with well-developed P-E

hysteresis loops. From Rayleigh analysis and aging studies, it was concluded that the high relative permittivity in these samples (compared to those cold sintered with lead nitrate) was due to a larger reversible contribution. Even though the liquid phase sintering process by Corker et al. using a CuO-PbO sintering aid can provide better densities at the same processing temperatures, the cold sinter-assisted process presented in this work shows that comparable dielectric and piezoelectric properties can be obtained in PZT ceramics. Furthermore, this work can be extended to composite systems where reactive sintering aids such as CuO-PbO can invoke undesirable chemical reactions or unwanted residue at the grain boundaries.

## ACKNOWLEDGMENTS

This material is based upon work supported by the National Science Foundation, as part of the Center for Dielectrics and Piezoelectrics under Grant Nos. IIP-1841453 and IIP-1841466. The authors appreciate the support from Dr. Richard Floyd and Dr. Jon-Paul Maria for sharing the design of their hydraulic press, and Tim Klinger for helping assemble the hydraulic press. The authors also thank Jeff Long for his help in making Rayleigh measurements. The authors gratefully acknowledge the extremely helpful comments of the anonymous reviewers.

## ORCID

*Shruti Gupta* https://orcid.org/0000-0003-0709-4241
*Dixiong Wang* https://orcid.org/0000-0002-2067-3646
*Clive A. Randall* https://orcid.org/0000-0002-5478-2699
*Susan Trolier-McKinstry* https://orcid.org/0000-0002-7267-9281

## REFERENCES

1. Ndayishimiye A, Largeteau A, Mornet S, Duttine M, Dourges M-A, Denux D, et al. Hydrothermal sintering for densification of silica. Evidence for the role of water. J Eur Ceram Soc. 2018;38(4):1860–70.
2. Chaim R, Shlayer A, Estournes C. Densification of nanocrystalline $Y_2O_3$ ceramic powder by spark plasma sintering. J Eur Ceram Soc. 2009;29(1):91–8.
3. Wu YJ, Li J, Kimura R, Uekawa N, Kakegawa K. Effects of preparation conditions on the structural and optical properties of spark plasma-sintered PLZT (8/65/35) ceramics. J Am Ceram Soc. 2005;88(12):3327–31.
4. Sharma PK, Ounaies Z, Varadan VV, Varadan VK. Dielectric and piezoelectric properties of microwave sintered PZT. Smart Mater Struct. 2001;10(5):878–83.
5. Atkin RB, Fulrath RM. Point defects and sintering of lead zirconate-titanate. J Am Ceram Soc. 1971;54(5):265–70.
6. Heidary DSB, Lanagan M, Randall CA. Contrasting energy efficiency in various ceramic sintering processes. J Eur Ceram Soc. 2018;38(4):1018–29.
7. Andrews A, Herrmann M, Shabalala TC, Sigalas I. Liquid phase assisted hot pressing of boron suboxide-materials. J Eur Ceram Soc. 2008;28(8):1613–21.
8. Miranzo P, González-Julián J, Osendi MI, Belmonte M. Enhanced particle rearrangement during liquid phase spark plasma sintering of silicon nitride-based ceramics. Ceram Int. 2011;37(1):159–66.
9. Vakifahmetoglu C, Anger JF, Atakan V, Quinn S, Gupta S, Li Q, et al. Reactive hydrothermal liquid-phase densification (rHLPD) of ceramics – a study of the $BaTiO_3[TiO_2]$ composite system. J Am Ceram Soc. 2016;99(12):3893–901.
10. Corker D, Whatmore R, Ringgaard E, Wolny W. Liquid-phase sintering of PZT ceramics. J Eur Ceram Soc. 2000;20(12):2039–45.
11. Wittmer DE, Buchanan RC. Low-Temperature densification of lead zirconate-titanate with vanadium pentoxide additive. J Am Ceram Soc. 1981;64(8):485–90.
12. Hayashi T, Inoue T, Nagashima Y, Tomizawa J, Akiyama Y. Low-temperature sintering of PZT with $LiBiO_2$ as a sintering aid. Ferroelectrics. 2001;258(1):53–60.
13. Saha AK, Kumar D, Parkash O, Sen A, Maiti HS. Effect of phosphorus addition on the sintering and dielectric properties of $Pb(Zr_{0.52}Ti_{0.48})O_3$. Mater Res Bull. 2003;38(7):1165–74.
14. Gutmanas EY, Lawley A. Cold sintering – a new powder consolidation process. Prog Powder Metall. 1983;39:1–15.
15. Maria J-P, Kang X, Floyd RD, Dickey EC, Guo H, Guo J, et al. Cold sintering: current status and prospects. J Mater Res. 2017;32(17):3205–18.
16. Guo HZ, Baker A, Guo J, Randall CA. Cold sintering process: a novel technique for low-temperature ceramic processing of ferroelectrics. J Am Ceram Soc. 2016;99(11):3489–507.
17. Guo J, Guo H, Baker AL, Lanagan MT, Kupp ER, Messing GL, et al. Cold sintering: a paradigm shift for processing and integration of ceramics. Angew Chem Int Ed. 2016;55(38):11457–61.
18. Randall CA, Guo J, Baker A, Lanagan M, Hanzheng GU, inventors. Penn State Research Foundation, United States patent application US 15/277,553. 2017 Mar 30.
19. Guo J, Berbano SS, Guo H, Baker AL, Lanagan MT, Randall CA. Cold sintering process of composites: bridging the processing temperature gap of ceramic and polymer materials. Adv Funct Mater. 2016;26(39):7115–21.
20. Herisson de Beauvoir T, Dursun S, Gao L, Randall C. New opportunities in metallization integration in cofired electroceramic multilayers by the cold sintering process. ACS Appl Electron Mater. 2019;1(7):1198–207.
21. Zhao X, Guo J, Wang K, Herisson de Beauvoir T, Li B, Randall CA. Introducing a ZnO-PTFE (polymer) nanocomposite varistor via the cold sintering process. Adv Eng Mater. 2018;20(7):1–8.
22. Pereira da Silva JG, Bram M, Laptev AM, Gonzalez-Julian J, Ma Q, Tietz F, et al. Sintering of a sodium-based NASICON electrolyte: a comparative study between cold, field assisted and conventional sintering methods. J Eur Ceram Soc. 2019;39(8):2697–702.
23. Wang D, Zhou D, Song K, Feteira A, Randall CA, Reaney IM. Cold-sintered C0G multilayer ceramic capacitors. Adv Electron Mater. 2019;5(7):1900025.
24. Nelo M, Siponkoski T, Kähäri H, Kordas K, Juuti J, Jantunen H. Upside – down composites: fabricating piezoceramics at room temperature. J Eur Ceram Soc. 2019;39(11):3301–6.
25. Wang D, Guo H, Morandi CS, Randall CA, Trolier-McKinstry S. Cold sintering and electrical characterization of lead zirconate titanate piezoelectric ceramics. APL Mater. 2018;6(1):016101.
26. Induja IJ, Sebastian MT. Microwave dielectric properties of mineral sillimanite obtained by conventional and cold sintering process. J Eur Ceram Soc. 2017;37(5):2143–7.

27. Grasso S, Biesuz M, Zoli L, Taveri G, Duff AI, Ke D, et al. A review of cold sintering processes. Adv Appl Ceram. 2020;1(1):1–29.
28. Kähäri H, Teirikangas M, Juuti J, Jantunen H. Dielectric properties of lithium molybdate ceramic fabricated at room temperature. J Am Ceram Soc. 2014;97(11):3378–9.
29. Kähäri H, Teirikangas M, Juuti J, Jantunen H. Improvements and modifications to room-temperature fabrication method for dielectric $Li_2MoO_4$ ceramics. J Am Ceram Soc. 2015;98(3):687–9.
30. Floyd RD Jr. Improving the instrumentation and science of cold sintering. Raleigh, NC: North Carolina State University. http://www.lib.ncsu.edu/resolver/1840.20/37232. Accessed 23 Jul 2019.
31. Wang D, Tsuji K, Randall CA, Trolier-McKinstry S. Model for the cold sintering of lead zirconate titanate ceramic composites. J Am Ceram Soc. 2020;103:4894–902.
32. Ham WK, Holland GF, Stacy AM. Low-temperature synthesis of superconducting $La_{2-x}M_xCuO_4$: direct precipitation from NaOH/KOH Melts. J Am Chem Soc. 1988;110:5214–5.
33. Friedman TL, Stacy AM. Electrochemistry in molten hydroxides: synthesis of $NaCuO_2$. J Solid State Chem. 1994;109:203–4.
34. Tsuji K, Ndayishimiye A, Lowum S, Floyd R, Wang KE, Wetherington M, et al. Single step densification of high permittivity $BaTiO_3$ ceramics at 300ºC. J Eur Ceram Soc. 2019;40(4):1280–4.
35. Sada T, Tsuji K, Ndayishimiye A, Fan Z, Fujioka Y, Randall CA. Enhanced high permittivity $BaTiO_3$–polymer nanocomposites from the cold sintering process. J Appl Phys. 2020;128(8):084103.
36. Ndayishimiye A, Sengul MY, Sada T, Dursun S, Bang SH, Grady ZA, et al. Roadmap for densification in cold sintering: chemical pathways. Open Ceramics. 2020;100019.
37. ASTM E112–13, Standard test methods for determining average grain size, ASTM International, West Conshohocken, PA; 2013.
38. Martinez-Casado FJ, Ramos-Riesco M, Rodriguez-Cheda JA, Cucinotta F, Matesanz E, Miletto I, et al. Unraveling the decomposition process of lead (II) acetate: anhydrous polymorphs, hydrates, and byproducts and room temperature phosphorescence. Inorg Chem. 2016;55(17):8576–86.
39. Floyd R, Lowum S, Maria J-P. Instrumentation for automated and quantitative low temperature compaction and sintering. Rev Sci Instrum. 2019;90(5):055104.
40. Svoboda J, Riedel H, Gaebel R. A model for liquid phase sintering. Acta Mater. 1996;44(8):3215–26.
41. Murray P, Rodgers EP, Williams AE. Practical and theoretical aspects of hot pressing of refractory oxides. Trans Br Ceram Soc. 1954;53(8):474–510.
42. Kingery WD, Woulbroun JM, Charvat FR. Effects of applied pressure on densification during sintering in the presence of a liquid phase. J Am Ceram Soc. 1963;46(8):391–5.
43. Felten EJ. Hot-pressing of alumina powders at low temperatures. J Am Ceram Soc. 1961;44(8):381–5.
44. PubChem [Internet]. Bethesda, MD: National Library of Medicine (US), National Center for Biotechnology Information; 2004. PubChem Compound Summary for CID 24924, Lead nitrate. https://pubchem.ncbi.nlm.nih.gov/compound/Lead-nitrate. Accessed 9 Dec 2020.
45. Jaffe B, Cook WR Jr, Jaffe H. Piezoelectric Ceramics. London, UK and New York: Academic Press; 1971.
46. Taylor DV, Damjanovic D. Evidence of domain wall contribution to the dielectric permittivity in PZT thin films at sub-switching fields. J Appl Phys. 1997;82(4):1973–5.
47. Mason WP. Aging of the properties of barium titanate and related ferroelectric ceramics. J Am Ceram Soc. 1955;27(1):73–85.
48. Yuhuan XU. Ferroelectric Materials and their Applications. Amsterdam, Netherlands: Elsevier; 2013.
49. Damjanovic D. Stress and frequency dependence of the direct piezoelectric effect in ferroelectric ceramics. J Appl Phys. 1997;82(4):1788–97.


## SUPPORTING INFORMATION

Additional supporting information may be found online in the Supporting Information section.

**How to cite this article:** Gupta S, Wang D, Randall CA, Trolier-McKinstry S. Comparison of different sintering aids in cold sinter-assisted densification of lead zirconate titanate. *J Am Ceram Soc*. 2021;104:5479–5488. https://doi.org/10.1111/jace.17934